Title

Discovery of Small Molecules for Fluorescent Detection of Complement Activation Product C3d

Journal

Journal of Medicinal Chemistry, 58(24)

ISSN

0022-2623

Authors

Gorham, Ronald D
Nuñez, Vicente
Lin, Jung-Hsin
et al.

Publication Date

2015-12-24

DOI

10.1021/acs.jmedchem.5b01062

Peer reviewed

Journal of Medicinal Chemistry

Article

pubs.acs.org/jmc

Discovery of Small Molecules for Fluorescent Detection of Complement Activation Product C3d

Ronald D. Gorham, Jr.,[†,∥,⊥] Vicente Nuñez,[†,#] Jung-Hsin Lin,[‡,§] Suzan H. M. Rooijakkers,[∥] Valentine I. Vullev,[†] and Dimitrios Morikis*[,†]

[†]Department of Bioengineering, University of California, Riverside, California 92521, United States

[‡]Division of Mechanics, Research Center for Applied Sciences and Institute of Biomedical Sciences, Academia Sinica, Taipei 115, Taiwan

[§]School of Pharmacy, National Taiwan University, Taipei 100, Taiwan

[∥]Department of Medical Microbiology, University Medical Center, Utrecht, 3584 CX Utrecht, The Netherlands

Supporting Information

ABSTRACT: Complement activation plays a major role in many acute and chronic inflammatory conditions. C3d, a terminal product of complement activation, remains covalently attached to cells and is an excellent biomarker of complement-mediated inflammation. We employed a virtual high-throughput screening protocol to identify molecules with predicted binding to complement C3d and with intrinsic fluorescence properties to enable detection. Pharmacophore models were developed based on known C3d−ligand interactions and information from computational analysis of structural and molecular dynamics data. Iterative pharmacophore-based virtual screening was performed to identify druglike molecules with physicochemical similarity to the natural C3d ligand CR2. Hits from the pharmacophore screens were docked to C3d and ranked based on predicted binding free energies. Top-ranked molecules were selected for experimental validation of binding affinity to C3d, using microscale thermophoresis, and for their suitability to become molecular imaging agents, using fluorescence spectroscopy. This work serves as a foundation for identifying additional fluorescent molecules with high-affinity for C3d that will subsequently be explored as noninvasive in vivo diagnostics of complement-mediated inflammation, for spatiotemporal monitoring of disease progression, and for targeting therapeutics to sites of inflammation.

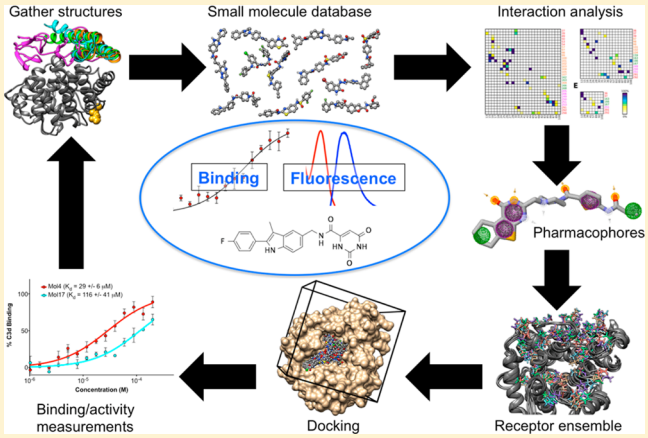

INTRODUCTION

The complement system plays a role in many autoimmune and inflammatory diseases.[1] Complement is considered a double-edged sword; it has evolved the capability to rapidly detect and eliminate pathogens but relies on coordination of complement regulator proteins to confer protection against host cell and tissue damage. Involvement of complement in autoinflammatory diseases stems from improper complement activation, dysregulation, or deficiency.[2] For example, mutations in complement regulator factor H lead to reduced complement regulation and increase the likelihood of developing both age-related macular degeneration and atypical hemolytic uremic syndrome. Alternatively, generation of autoantibodies (antibodies against self-antigens) and inadequate clearance of immune complexes result in classical pathway complement activation, which further exacerbates chronic inflammation resulting from these autoimmune diseases. Since complement is involved in most autoinflammatory diseases, levels of complement proteins (both precursors and activation products) are often correlated with disease state.[3,4] Measurement of serum levels of complement factors, however, often leads to misdiagnoses, since serum levels are highly variable in both healthy and diseased individuals.[4] Since complement activation is characterized by extensive covalent attachment of proteins to cell surfaces, a more reliable alternative involves measurement of complement activation products on affected tissues (Figure 1).[5,6] During complement activation, complement component 3 (C3) is cleaved, exposing a reactive thioester that can covalently link nascently generated C3b to cell surfaces. Further cleavage events yield C3d (the terminal cleavage product of C3), which remains covalently linked to cells long after complement activation[4] and has been explored and used for tracking disease progression in a number of conditions,

Received: July 7, 2015
Published: November 27, 2015

DOI: 10.1021/acs.jmedchem.5b01062
J. Med. Chem. 2015, 58, 9535−9545

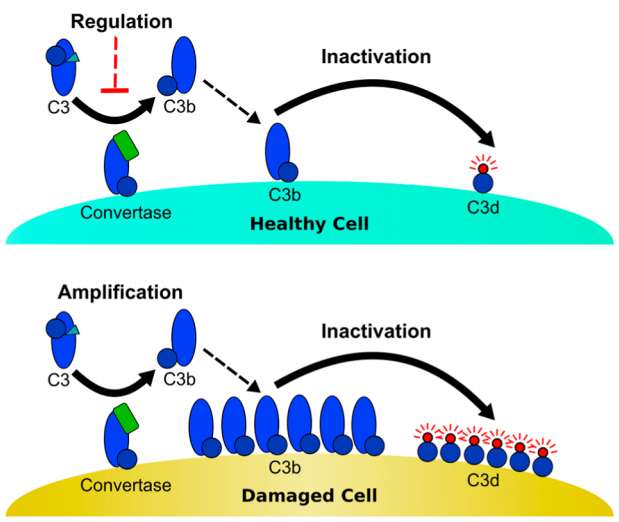

Figure 1. Overview of complement activation and regulation on healthy and damaged cells. Complement is activated, leading to production of active fragment C3b, which can covalently attach to cell surfaces via the C3d domain (dark blue circle). Under normal conditions, complement regulators prevent further cleavage of C3 to C3b by convertase enzymes and eventually inactivate cell-bound C3b molecules by cleavage to C3d. When complement is dysregulated or under inflammatory conditions, C3b is rapidly amplified on cell surfaces, and subsequent C3b cleavage events lead to an accumulation of C3d, the long-lived biomarker of complement activation. The red beacon attached to C3d symbolizes fluorescent small molecules that can detect sites of complement-mediated inflammation.

including neurological (Alzheimer's disease and multiple sclerosis),[7] renal (lupus nephritis, glomerulonephritis, and atypical hemolytic uremic syndrome),[8,9] ocular (age-related macular degeneration),[10] and systemic (systemic lupus erythematosus, rheumatoid arthritis, and chronic obstructive pulmonary disease)[4,11−14] diseases and xenotransplantation.[2] However, measurement of C3d levels typically requires tissue biopsies.[5,6,9,15] It is therefore desirable to develop a noninvasive method to detect levels of complement activation fragments on tissues.

Many groups have attempted to develop molecules that target C3d for diagnosis and treatment of complement-mediated diseases. C3d is a marker for complement activation but also functions to stimulate B cell activation and production of antibodies through its interaction with complement receptor 2 (CR2).[16−18] Indeed, several studies have shown that molecular therapeutic agents (i.e., soluble complement regulators or antibodies that downregulate complement activation) targeting sites of complement activation (i.e., where C3d has deposited) via CR2 can locally inhibit complement activation, resulting in a more efficient therapeutic while simultaneously minimizing susceptibility to infections.[19−24] Recently, two groups have pursued development of noninvasive molecular diagnostics for C3d. Serkova et al. developed iron oxide nanoparticles conjugated with portions of CR2, which targeted the particles to C3d. They were able to detect renal C3d deposits in mouse models of lupus nephritis using MRI.[9] Thurman et al. generated fluorescently conjugated monoclonal antibodies that specifically bound C3d with high affinity and successfully imaged C3d on the retina of mice in vivo.[5] While these two studies represent significant advances, it would be beneficial to formulate C3d diagnostics using non-protein chemical compounds. Small chemical compounds offer many advantages in context of molecular diagnostics and therapeutics. They have higher bioavailability than larger protein-based therapeutics, are less prone to degradation, and are more cost-effective to produce. Since most complement-targeted molecules are proteins, development of small molecules represents a major step forward.

Herein, we describe the discovery of C3d-binding small fluorescent molecules. We used a comprehensive virtual high-throughput screening (vHTS) protocol to search over seven million druglike small molecules for predicted binding to C3d. Experimental binding studies led to the identification of 10 molecules that bind to C3d, with affinities ranging from 1 to 500 μM. Three of these compounds are strongly fluorescent, exhibiting emission quantum yields (Φ_{fl}) larger than 0.2. Additionally, at least one molecule exhibits a substantial enhancement in fluorescence in the presence of C3d. These findings provide an important foundation for the development of theranostic molecules for detection and treatment of complement-mediated inflammation in vivo.

RESULTS

Virtual High-Throughput Screening Protocol. We employed a multistep virtual high-throughput screening framework to efficiently screen more than 7 million commercially available druglike compounds for predicted C3d binding (Figure 2). Our screen was guided by known structural,

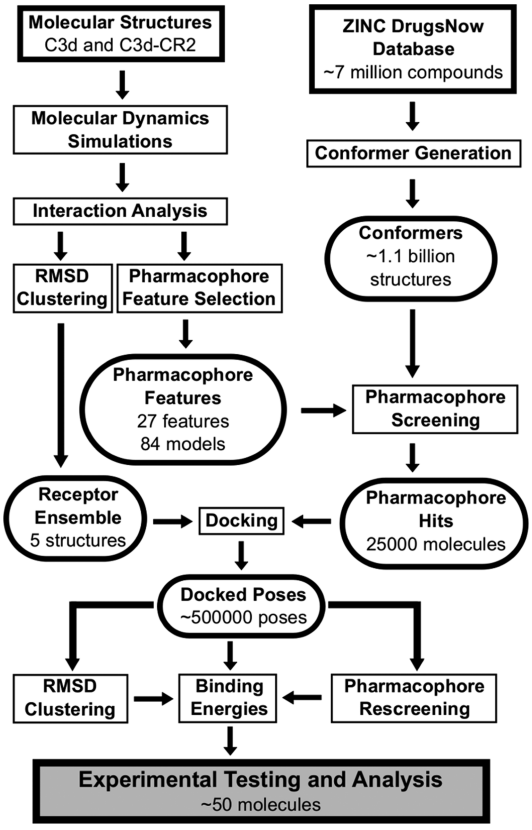

Figure 2. Overview of virtual high-throughput screening framework. Required inputs are shown in the top boxes (white with dark outline), computational methods in white boxes with light outline, and intermediate outputs in white ovals. The framework leads to selection of molecules for experimental testing, shown in the gray box at the bottom.

DOI: 10.1021/acs.jmedchem.5b01062
J. Med. Chem. 2015, 58, 9535−9545

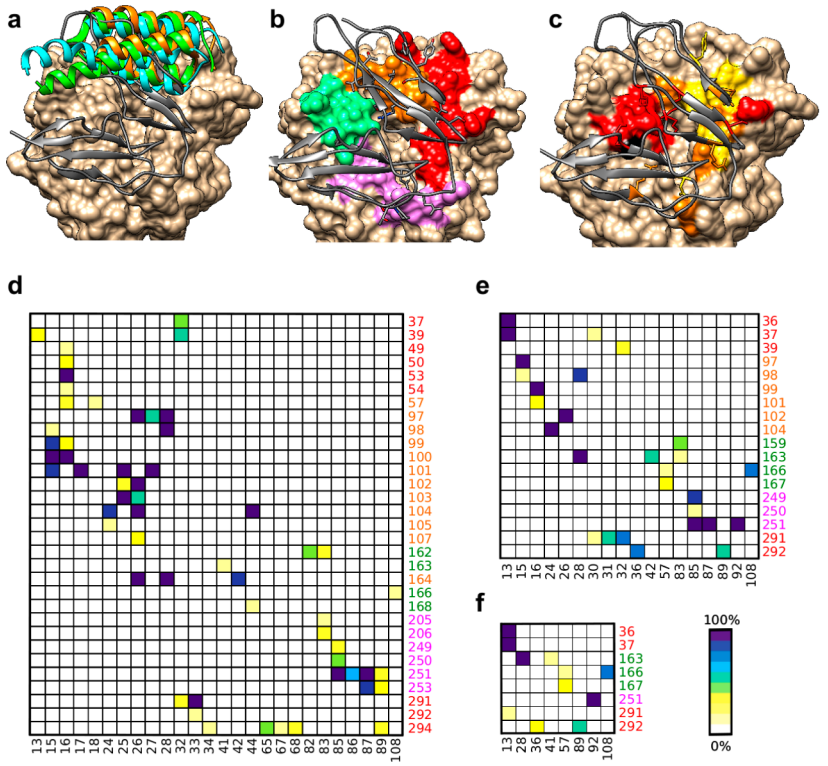

Figure 3. Analysis of C3d−ligand interactions. (a) The molecular graphic shows superimposed cocrystal structures of C3d (tan) in complex with Efb-C (green), Ecb/Ehp (orange), Sbi-IV (cyan), and CR2 (gray). The location of the thioester (for cell surface attachment) is on the back side of C3d. (b) Examination of intermolecular interactions of C3d (tan) with CR2 (gray ribbon) reveals a ring of interactions surrounding a deep cavity on the C3d surface. The figure shows interacting regions of C3d, divided into four sectors; acidic cluster 1 (red), nonpolar cluster (orange), acidic cluster 2 (green), and polar cluster (purple). (c) The C3d surface (tan) and CR2 side chains are colored by their effect on experimental binding affinity compared to the wild-type C3d−CR2 complex:[30] <25% binding (red), 25−59% binding (orange), 60−84% binding (yellow), and >125% binding (black). C3d−CR2 interaction occupancies were calculated throughout a 20 ns MD trajectory, and nonpolar interactions (d), hydrogen bonds (e), and salt bridges (f) are shown here. CR2 residues are on the *x*-axes, and C3d residues are on the *y*-axes. C3d residue labels are colored according to their corresponding sector (from panel b).

computational, and experimental data regarding C3d and C3d−ligand interactions. First, we performed MD simulations of free C3d and the C3d−CR2 complex and analyzed interactions and conformational flexibility in each trajectory. Interaction data, in conjunction with available experimental mutagenesis data for C3d and CR2, were used to define pharmacophore features and derive sets of pharmacophore models for the initial compound screen. We generated conformers of ZINC compounds in order to account for compound flexibility and screened these conformers against 84 pharmacophore models, yielding ∼25 000 unique compounds that matched three or more pharmacophore features in at least one model. Each of the pharmacophore hits was docked to five distinct conformations of C3d, derived from rmsd based clustering of binding site residues from MD trajectory snapshots of C3d, both free and in complex with CR2. Lowest energy binding poses for each molecule (and their corresponding binding energies) were reported. Since molecules were free to dock anywhere within the C3d−CR2 binding cavity, many binding poses varied considerably from one another. We used rmsd clustering of poses to identify compounds that docked in a similar conformation to all receptor conformations. Furthermore, we rescreened docked poses against pharmacophore models to identify compounds that exhibited low energy binding and desired physicochemical property distribution simultaneously.

C3d−Ligand Interaction Analysis. C3d is a molecular hub for both host and pathogenic proteins. Interestingly, the majority of known C3d ligands bind at a concave acidic face of the molecule, opposite the reactive thioester responsible for cell surface attachment (Figure 3a).[25] We leveraged the wealth of structural, biochemical, and biophysical data on these interactions[26−36] to guide our search for C3d-binding small molecules. Interestingly, all of the crystallographic structures of C3d (free and complexed) have a deep cavity preserved in the center of the acidic face. Since the rest of C3d has a relatively flat or convex surface, this cavity represents an attractive target for small molecule binding. While many ligands bind C3d at the acidic face, CR2 binds entirely over the cavity on its surface (Figure 3b,c). Thus, we focused on C3d−CR2 interaction for our small molecule screen.

We performed MD simulations of the C3d−CR2 complex in order to evaluate the conformational flexibility of the C3d−CR2 binding site and to elucidate which residues are crucial to the C3d−CR2 interaction. Similar to most known ligands of C3d, CR2 binds at the concave acidic region of C3d (Figure 3b,c), and binding is dominated by electrostatic interactions. Through initial examination, a deep cavity is observed in the concave acidic region of C3d, and this cavity persists during MD simulations of both free C3d and the C3d−CR2 complex. Interestingly, CR2 itself does not "enter" the cavity but rather resides atop the cavity, forming polar and nonpolar interactions with a ring of C3d residues lining the perimeter of the cavity (Figure 3b). The C3d interaction ring can be divided into four sectors, based on physicochemical interaction type and spatial

DOI: 10.1021/acs.jmedchem.5b01062
J. Med. Chem. 2015, 58, 9535−9545

distribution. Sectors 1 (red) and 3 (green) consist primarily of electrostatic interactions, while sectors 2 (orange) and 4 (purple) are involved in hydrogen bonding and nonpolar interactions. Residues in sectors 1−3 are also crucial for interactions between C3d and staphylococcal virulence factors Efb-C, Ecb, and Sbi-IV, all of which have been shown (both structurally and functionally) to competitively inhibit C3d−CR2 interaction (Figure 3a). Thus, since these C3d residues are critical for binding of multiple natural ligands, they represent important targets for identification and design of potential diagnostic and therapeutic molecules.

The interaction between C3d and CR2 has been well studied in the past decade. A large amount of mutagenesis data are available, which facilitated our vHTS efforts.[30] Single amino acid mutations of C3d and CR2, and their relative effects on binding, are shown in Figure 3c. There are five red (<25% WT binding activity), four orange (25−59% WT binding activity), and four yellow (60−84% WT binding activity) mutations of C3d and five red, three orange, and two yellow mutations of CR2. Concentration of similar colors in the same area points to the importance of specific regions of the interface in binding, with weaker contribution of surrounding areas. There is one enhancing mutation of C3d (black) within the C3d−CR2 interface. The fact that the enhancing mutation was a lysine to alanine mutation, while all mutations of negatively charged residues of C3d inhibited binding, strongly supports the importance of electrostatic interactions at this C3d−CR2 interface. Naturally, the locations of inhibitory mutations (red, orange, and yellow) correspond to the ring of interactions seen in Figure 3b. Whereas inhibitory mutations are spatially disbursed, we noticed that the most inhibitory mutations (red) are observed in sectors 1 and 3. Therefore, while all persistent interactions from MD simulations were considered during vHTS of C3d (Figure 3d−f), charge−charge interactions (Figure 3f) were given special consideration in development of pharmacophore models and postprocessing/reranking of lead compounds after docking.

Pharmacophore Screening. The next step in our vHTS protocol involved searching for molecules with similar geometric and spatial arrangement of physicochemical properties to CR2. We implemented a dynamic pharmacophore modeling approach, inspired by previous work.[37−39] On the basis of the MD simulation of C3d−CR2 and previous experimental mutagenesis data, we selected several CR2 residues important for its interaction with C3d (Figure 4a). The arrangement of selected functional moieties (isolated from CR2 residues) is shown in Figure 4b, with respect to C3d. These moieties were used to define 24 pharmacophore features of varying types (i.e., positive, negative, hydrogen bond acceptor or donor, aromatic, hydrophobic), based on the physicochemical properties of each moiety itself (Table S1 and Figure 4c). Since these atoms fluctuated to varying degrees over time, tolerance spheres were generated with radii large enough to incorporate 95% of their occupied positions. In addition, three aromatic features were defined and manually placed in the bottom of the C3d cavity in order to "anchor" small molecules into the cavity.

We selected pharmacophore models from subsets of the 27 features in order to optimize the number of hits, specificity, and screen time. The first parameter in model selection was the number of pharmacophore features. Using too few features often yields large numbers of false positives in pharmacophore screens, whereas using too many features may be too stringent

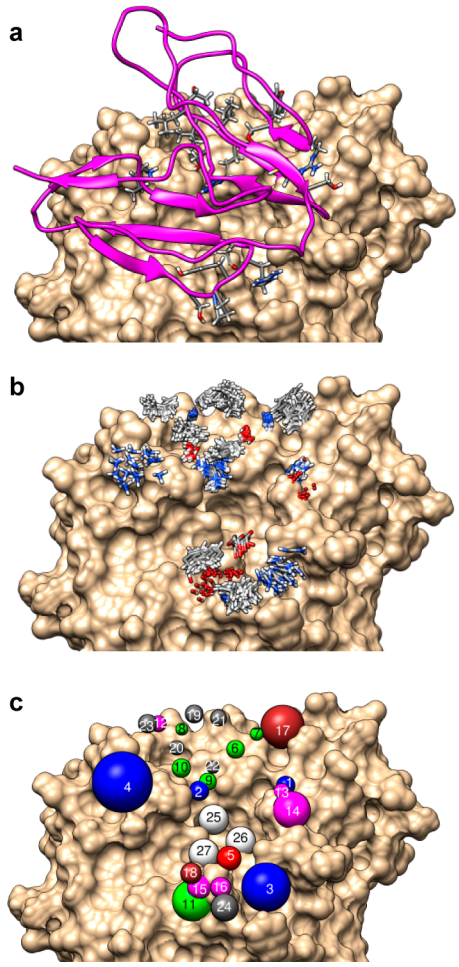

Figure 4. Development of a dynamic pharmacophore model based on C3d−CR2 interaction. (a) C3d (tan surface) is shown in complex with CR2 (magenta ribbon), with interacting side chains of CR2 shown as sticks colored by element type (carbon, gray; nitrogen, blue; oxygen, red; hydrogen, white). (b) Positions of chemical groups from CR2 residues interacting with C3d are shown at 10 different time points during the 20 ns MD trajectory. The physicochemical properties and spatial distribution of the atom groups were used to define the 27 pharmacophore features observed in (c). Features are colored by pharmacophore type (hydrogen bond donor, green; hydrogen bond acceptor, magenta; positive charge, blue; negative charge, red; aromatic, brown; hydrophobic, gray).

during the search, yielding few or no hits at all. Selected pharmacophore models contained between three and five features, achieving a balance between specificity and diversity in molecule hits. Since the interfeature distances in our initial model are quite variable, we also applied distance criteria in model selection. Selected models had interfeature distances of at least 4 Å and less than 15 Å. These criteria alleviate fortuitous matching of multiple features by a single chemical moiety while constraining the search to distances that can reasonably be spanned by a druglike small molecule (MW < 500). Finally, we restricted model selection based on properties of specific features. Models were selected to contain one hydrophobic feature from the cavity base (feature 25, 26, or 27), one positive feature (feature 1, 2, 3, or 4), one feature representing a crucial interaction based on experimental binding data (feature 1, 2, 5, 6, 9−11, 13−16, 18, 20, 22, or 24), and no more than one additional hydrophobic feature (Table S1). These criteria result

DOI: 10.1021/acs.jmedchem.5b01062
J. Med. Chem. 2015, 58, 9535−9545

in physicochemically diverse pharmacophore models that explore multiple regions of the C3d−CR2 interaction site.

In total, 84 pharmacophore models were selected, and generated conformers for ZINC compounds were screened against each model. We found that three-feature models were highly nonspecific and yielded very large numbers of hits. Models containing features from sector 4 also yielded large numbers of hits, likely because of the close proximity of features to each other and to required hydrophobic base features. Since sector 4 is less important than other sectors for C3d−ligand interactions, we focused on models comprising features from sectors 1−3, with either four or five features. We narrowed the search to 51 models (27 of which yielded at least 1 hit), resulting in a total of 25 668 unique compounds. Indeed, some models accounted for a larger number of hits than others. Among the 27 models with at least one hit, the number of hits ranged from 1 to 17 458, with a median of 47 and mean of 972. Thus, most of the models had a small number of hits. Models with the highest number of hits involve features derived from sector 2 interactions, with some shared features from either sector 1 or 3 (the most represented features were features 1, 2, 6, and 25). These pharmacophore hits are likely representative of C3d−ligand interactions in general, since most known C3d ligands bind to sectors 1−3.

Docking and Postprocessing. It is well-known that incorporation of target protein flexibility improves the accuracy of docking simulations.[40,41] However, accounting for ligand-induced conformational change in the target binding site is not feasible for large numbers of molecules with current computational resources. As an alternative, one can dock small molecules to a structurally diverse ensemble of target protein conformations in order to increase the probability of encountering a binding site conformation resembling the conformation of the ligand-bound state. We followed a protocol similar to the relaxed complex scheme (RCS),[42,43] which has been used previously to successfully identify small molecules that bind to specific protein targets.[44] We docked molecules to a conformational ensemble of C3d to implicitly incorporate receptor flexibility into docking simulations. From MD simulations of free C3d and the C3d−CR2 complex, we clustered C3d structures based on rmsd of interacting residues, as determined from the C3d−CR2 MD simulation (Figure 3d−f). This method allowed for selection of C3d structures with the most diverse CR2 binding modes. We obtained five structures, with rmsd for binding site residues between 2 and 3 Å for all structure pairs. The low pairwise rmsd values indicate robust structure within the binding site. Figure 5 shows the superposition of the five selected C3d structures from rmsd clustering, which shows similar positions for side chains of CR2-interacting residues, regardless of whether C3d is free or complexed.

Since we are exploring a large protein−protein interface as the molecular target in this vHTS project, it is of interest to examine where compounds dock within the entire binding site. Thus, during docking simulations, we allowed compounds to dock within a large (40 Å × 40 Å × 40 Å) grid surrounding the acidic concave region of C3d (Figure 5). Molecules were docked to the five C3d conformations mentioned above, and predicted binding energies were reported for low-energy docked poses, based on the AutoDock Vina scoring function.

While many docked poses had low predicted binding energies (as low as −10.1 kcal/mol), some compounds bound strongly to a small number of C3d conformations and poorly to others. Some molecules docked in very different orientations to different C3d conformations, and others docked deep in the C3d cavity such that inhibition of CR2 binding would be improbable. We clustered low energy compounds, based on rmsd of their docked conformations to the five diverse C3d structures, and identified compounds that had similar molecule binding modes (<5 Å rmsd) to all five structures. Additionally, we rescreened all docked poses against the pharmacophore models used in the initial screening round by checking whether molecule docked poses had chemical groups that overlapped with pharmacophore features. We selected compounds that matched a combination of at least two pharmacophore features while docked to at least three different C3d structures. We selected a list of hits with <−6.8 kcal/mol mean binding energy (corresponding to K_D = 10 μM at room temperature) that met the rmsd and pharmacophore postprocessing criteria, yielding 14 compounds. In addition, we selected additional compounds that met rmsd criteria with energies of <−8.0 kcal/mol, as top-binding compounds. A total of 49 compounds were selected for experimental evaluation (Table S2).

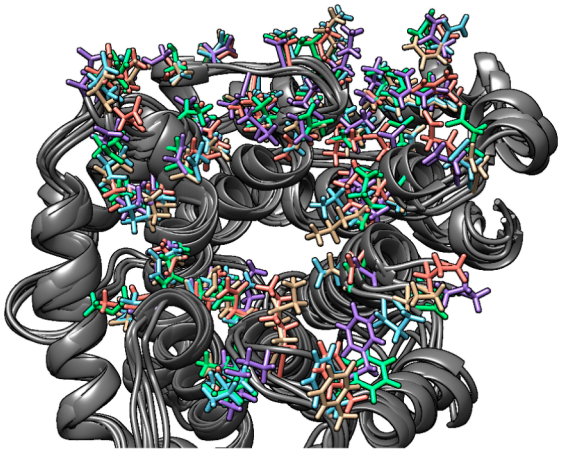

Figure 5. C3d conformational ensemble from 20 ns MD simulation and rmsd-based clustering. Residue side chains used for rmsd clustering criteria are shown as sticks, and the different colors correspond to conformations of the side chains in five different receptor structures.

Experimental Evaluation of C3d Binding. In order to validate our hits from vHTS, we measured binding of 49 selected compounds using microscale thermophoresis. All molecules were tested in a concentration-dependent manner, starting at 200 μM concentration (most molecules were poorly soluble in aqueous solution above this concentration). We identified nine molecules that bind to C3d, with binding affinities (K_D) ranging between 25 and 500 μM. The molecular structures and binding curves for top molecules are shown in Figure 6, and other binding molecules are shown in Supporting Information Figure S1.

Absorption and Fluorescence Properties. Our ultimate goal is to design small molecules that can be used for optical detection of C3d on tissues in vivo, e.g., a small molecule that can serve as a contrast agent for fluorescence imaging of regions in tissues with high levels of bound C3d. Since all C3d-binding molecules contain small aromatic moieties and functional groups that mediate extended π-conjugation, we expected that the molecules themselves might exhibit intrinsic fluorescence. Thus, we evaluated the photophysical properties of C3d-

DOI: 10.1021/acs.jmedchem.5b01062
J. Med. Chem. 2015, 58, 9535−9545

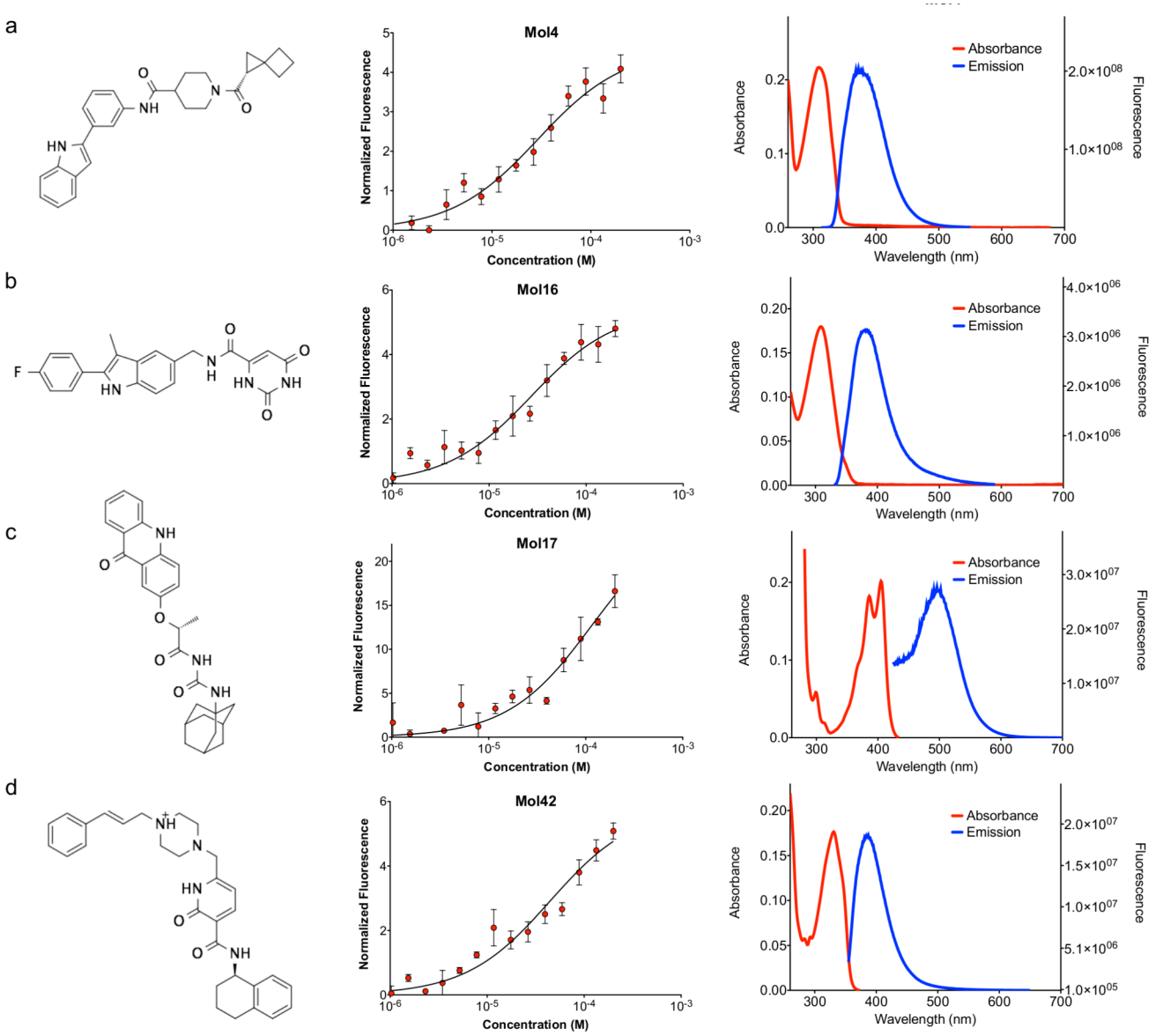

Figure 6. Chemical structures, binding, and fluorescence data for four top-performing molecules from virtual high-throughput screen. Data are shown for Mol4 (a), Mol16 (b), Mol17 (c), and Mol42 (d). Chemical structures are shown in the left panels, concentration-dependent thermophoresis binding curves in the center panels, and absorption and emission spectra in the right panels.

binding compounds to determine their diagnostic potential. We examined the absorption and fluorescence properties of nine C3d-binding compounds in order to determine if optical detection is feasible. All molecules exhibit pronounced absorption in the UV region and/or the blue edge of the visible spectrum (Figures 6 and S1). Eight of the nine examined C3d-binding compounds exhibit fluorescence with emission quantum yields ranging from about 0.001 to nearly unity (Table 1). As expected, the fluorescence spectra of the compounds containing quinolone moieties, such as Mol22 and Mol36, span between about 400 and 550 nm (Figure S1). Similarly, the indole-containing compounds, such as Mol4, Mol5, and Mol16, fluoresce between about 300 and 450 nm (Figures 6 and S1). The acridone derivative, Mol17, stands out with intense visible fluorescence and Φ_{fl} close to unity (Table 1, Figure 6).

Since many of these molecules have fluorescence spectra that overlap with tryptophan, we examined their fluorescent properties using longer wavelength (i.e., off-peak) excitation. When molecules were excited at 350 nm, in general we observed a reduction in fluorescence quantum yield (Table S3). Also, since many of the molecules have weak absorption at 350

Table 1. Binding and Fluorescence Properties of Nine C3d-Binding Compounds

Mol	K_D (μM)	excitation peak (nm)	emission peak (nm)	quantum yield
4	29 ± 8	315	380	0.560
5	68 ± 14	280	400	0.260
11	45 ± 13	310	405	0.001
16	27 ± 5	310	385	0.002
17	116 ± 41	390/405	500	0.984
22	183 ± 81	355	455	0.044
35	417 ± 171	275	460	0.001
36	132 ± 28	320	425	0.017
42	45 ± 15	335	390	0.011

DOI: 10.1021/acs.jmedchem.5b01062
J. Med. Chem. 2015, 58, 9535−9545

nm, highly concentrated solutions led to anomalous effects in fluorescence spectra, likely due to molecule aggregation. Excitation at 320 or 330 nm helped to reduce tryptophan fluorescence while simultaneously maintaining adequate fluorescence emission from the molecules (i.e., Mol4 and Mol16).

We also evaluated the fluorescence properties of top-performing molecules in the presence of C3d. Often, when small molecule fluorophores bind to their targets, fluorescence may be quenched, an undesirable property for potential diagnostic molecules. In the presence of increasing concentrations of C3d, no significant quenching was observed for any of the tested molecules. Remarkably, Mol4 underwent drastic fluorescence enhancement in the presence of C3d, with up to 5-fold higher fluorescence at subsaturating concentrations of C3d (Figure 7).

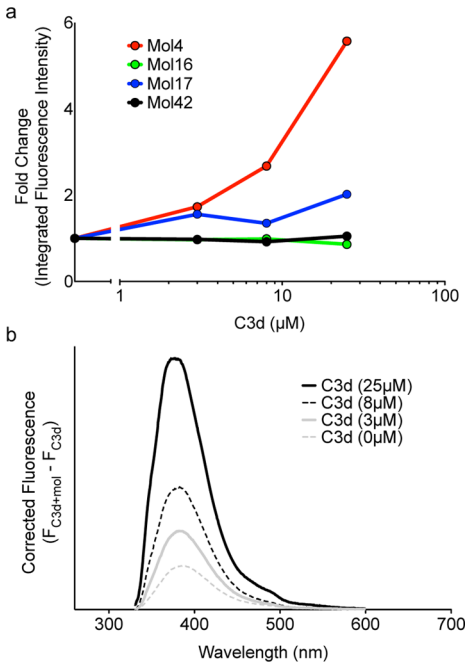

Figure 7. Fluorescence of top-performing molecules in the presence of C3d. (a) The fold-change in integrated fluorescence emission intensity is shown as a function of C3d concentration for Mol4, -16, -17, and -42. The fold change is the ratio of integrated fluorescence emission intensity at each C3d concentration to that of the molecule alone (0 μM C3d). (b) Corrected fluorescence emission spectra of Mol4 in the presence of 0, 3, 8, and 25 μM C3d.

Iterative Molecule Improvement. On the basis of the results of the initial virtual screen, and the identification of C3d-binding molecules via microscale thermophoresis, we sought to improve C3d binding affinity. We used the structures of these nine top molecules to identify additional molecules with structural similarity. Furthermore, due to issues with poor molecule solubility, we incorporated an additional filter for predicted log P values (log P < 3) to eliminate very hydrophobic molecules from our search. Finally, we docked our new set of molecules to 40 distinct C3d conformations, selected from MD simulations in the same manner as the original five conformations. We selected molecules with highest affinities to single C3d conformations and highest mean binding affinities (to all C3d conformations), keeping all molecules that were predicted to bind as well or better to C3d as compared to our hits from the first round of screening and binding. From this screen, we identified a molecule with 15-fold improved affinity (K_D = 1.7 μM) compared to the top molecule from the initial screen (Figure 8).

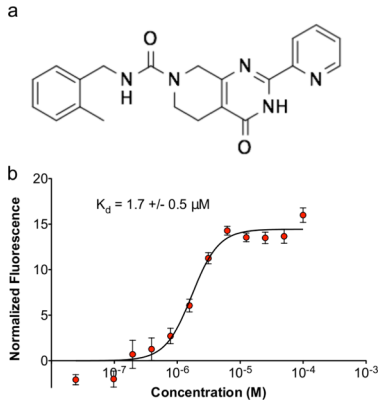

Figure 8. Chemical structure (a) and concentration-dependent thermophoresis binding curve (b) for top C3d-binding molecule (Mol68) from second iteration of virtual screening.

DISCUSSION

Excessive and inappropriate complement activation often plays an integral role in the development and progression of autoinflammatory conditions. Many recent efforts have focused on development of complement-targeted therapeutics and diagnostics, which can effectively regulate and detect complement-mediated inflammation. Indeed, two therapeutics are currently on the market for treatment of complement-related diseases, and many more are in the pipeline.[6] Additionally, fluorescently labeled monoclonal antibodies are being developed for in vivo detection of complement-mediated inflammation.[5] However, the majority of these molecules are biopharmaceuticals, which are expensive to produce, are difficult to deliver, and exhibit poor in vivo stability and bioavailability. It is desirable to identify small druglike complement diagnostic and therapeutic molecules to overcome these challenges. While complement activation is dependent on enzymatic cleavage of complement components, propagation of the cascades relies primarily on large protein complexes, which comprise expansive and topographically flat interfaces that lack defined cavities for small molecule binding. As a consequence, few small molecules that bind or inhibit complement have been identified, and all of these bind to enzyme active sites or GPCRs, which represent traditional targets for small druglike chemical compounds.

In this work, we successfully identified several small molecules that bind to complement fragment C3d. To our knowledge, these are the first small molecules known to bind to a nontraditional drug target (enzymes and GPCRs) of complement. Furthermore, this is the first virtual screen to successfully identify small molecules that bind to complement. In the first round, we identified nine molecules (from 50 total tested) that bound to C3d with 25−450 μM affinity. Subsequently, we used the structures of these molecules as a basis for a second round of virtual screening to identify additional C3d-binding molecules with higher affinity. Indeed, we identified a molecule with 1.7 μM binding affinity, a 15-fold improvement over top molecules from the first round.

DOI: 10.1021/acs.jmedchem.5b01062
J. Med. Chem. 2015, 58, 9535−9545

The successful identification of several binding molecules demonstrates the efficacy of our virtual screening framework and opens the door to future small molecule screening against a wide variety of complement targets, aimed toward both detection and inhibition. However, we must exercise caution in proceeding with further screening and optimization, in order to avoid challenges encountered in the initial stages. Our virtual screening protocol utilized pharmacophore models to initially filter ∼7 million molecules down to ∼25 000, which was a much more manageable number for more rigorous docking simulations. Despite successful identification of molecules via this procedure, it is critical to evaluate the accuracy of our pharmacophore modeling strategy. We found that many docked poses did not align well with their original pharmacophore models. Only 36% of the initial pharmacophore hits matched at least two pharmacophore features (from any model) after docking and rescreening. In fact, none of the pharmacophore rescreen hits bound to C3d in vitro (Table S2, Mols B1−B42 vs B43−B49). This suggests that the pharmacophore models should be adapted for future screens and further optimization, based on our lead compounds.

Through examination of the docked binding poses of the 10 C3d-binding molecules, it is evident that, in general, all molecules bind in and around the deep cavity in the C3d surface (Figure S2). There is great diversity in binding modes (even among different poses of a single molecule), but most molecules occupy the center of the cavity and stretch either through the "channels" that run southwest or southeast from the central cavity, or upward along the wall into sectors 2 and 3 (northwest from the central cavity). These molecules share conserved hydrogen bonding interactions, mediated by several key C3d residues surrounding the central cavity (Figure S3). Interestingly, although we set out to identify molecules that interacted with C3d in a similar manner to CR2, most molecules bound deep within the C3d cavity. Thus, future efforts should focus on the cavity and channels of C3d, at least for potential diagnostic molecules, where binding (and not inhibition) is sufficient. On the basis of the structures of C3d-binding molecules and analysis of molecule docking, we can redesign pharmacophore models for further structure-based optimization. Figure S4 shows the surface of C3d with seven mock pharmacophore features, representing important hydrophobic contacts and hydrogen bonding interactions conserved largely among C3d-binding molecules. In conjunction, more precise determination of molecule binding mode, via extensive molecular dynamics simulations, NMR, or optimally crystallographic structures of C3d−ligand complexes, will facilitate further structure-based optimization. This information can be used to improve molecule binding to C3d.

The molecules described in this work provide a foundation for the development of small molecule diagnostics of complement-mediated inflammation. In addition to binding to C3d, many of these molecules exhibit intrinsic fluorescent properties. Another challenge concerns fluorescent detection of C3d-binding molecules. Most of the molecules described in this work have peak excitation wavelengths in the UV spectrum, with little to no absorption past 350 nm. This poses a problem, as many biomolecules in cells and tissues exhibit autofluorescence in this wavelength regime. One molecule (Mol17) is excitable at 405 nm and emits around 500 nm but only weakly binds C3d. Indeed, we noticed that at 310 nm excitation, there is indeed very high fluorescence emission due to C3d alone. In contrast, excitation at 350 nm drastically reduces tryptophan fluorescence but often requires much higher molecule concentrations and can diminish molecule quantum yield. However, even shifting only to 320 or 330 nm drastically reduced the background fluorescence. Thus, these wavelengths may be appropriate for exciting some of our lead molecules that still have sufficient absorption in this range.

Additionally, intrinsic fluorescence of unbound molecule is an obstacle to C3d detection as well, as it may be difficult to distinguish from the signal of C3d-bound molecule. It is thus desirable for molecules to undergo a significant increase in quantum yield upon C3d binding. We identified at least one molecule (Mol4) that exhibited 5-fold enhanced fluorescence in the presence of C3d. It is possible to utilize chemical features of top-binding molecules, in conjunction with specific fluorescent chemical groups, to design new molecules with more desirable binding and photophysical properties. Finally, further experimental work is required to determine molecule binding specificity and the ability to detect C3d in native biological environments, both ex vivo (inflammatory cell culture models) and in vivo.

METHODS

MD Simulations. Explicit solvent MD simulations were performed for C3d and C3d−CR2 using NAMD.[45] Crystallographic structures of C3d (PDB code 1C3D) and C3d−CR2 (PDB code 3OED) were obtained from the Protein Data Bank (PDB).[46] Missing heavy atoms and hydrogens were added, and molecules were parametrized using the CHARMM27 force field,[47] in VMD.[48] Structures were placed in TIP3P water cubes, with a minimum distance of 12 Å between any protein atom and the cube boundary, and sodium and chloride counterions were added to achieve 150 mM ionic strength and neutralization of protein charges. Each system was energy minimized using 25 000 steps of conjugate gradient minimization, followed by heating and equilibration steps. After minimization, all protein atoms were harmonically constrained. A force constant of 10 kcal mol^{-1} $Å^{-2}$ was used during heating (62 ps) and the first equilibration stage (50 ps), followed by three equilibration stages (50 ps each) using force constants of 5, 2, and 1 kcal mol^{-1} $Å^{-2}$, respectively. In the final equilibration stage (50 ps), only backbone atoms were constrained (at 1 kcal mol^{-1} $Å^{-2}$). Equilibrated systems were simulated for 20 ns with no harmonic constraints. In all simulations, periodic boundary conditions and particle mesh Ewald electrostatics were employed, with nonbonded interaction cutoff and switching distance of 12 and 10 Å, respectively. Bonds involving hydrogen atoms were fixed using SHAKE, and 2 fs integration time steps were used. Langevin temperature and pressure controls were used for all NPT ensemble simulations.

Dynamic Pharmacophore Models. The MD trajectory of C3d−CR2 was used to develop dynamic pharmacophore models. The trajectory was analyzed using the Bio3D package[49] in R and UCSF Chimera,[50] and occupancies of nonpolar interactions, hydrogen bonds, and salt bridges were calculated. CR2 residues participating in persistent intermolecular salt bridges, hydrogen bonds, or nonpolar interactions (>50% occupancy) were selected as tentative pharmacophore points. Atoms of the relevant chemical groups in each selected residue were identified, and mean positions of centers of mass were calculated. A freestyle pharmacophore hypothesis was generated using Phase,[51,52] with 24 features corresponding to mean center-of-mass positions of specified CR2 residues. Feature types were defined based on the physicochemical properties of the CR2 atoms used to select them. The conformational flexibility (positional variability) of each feature was calculated from the MD trajectory and used to define the tolerance radii of each corresponding feature of the pharmacophore model. Additionally, three hydrophobic/aromatic features were manually placed at the bottom of the C3d cavity in order to "anchor" small molecules deep within the C3d cavity to facilitate energetically favorable binding. From a total of 27 pharmacophore features, subsets

DOI: 10.1021/acs.jmedchem.5b01062
J. Med. Chem. 2015, 58, 9535−9545

of 3−5 features were defined, using interfeature distances, diversity of feature types, and experimental mutagenesis/binding/functional data as selection criteria. A total of 84 pharmacophore models were selected for screening. The source of screening molecules in this study was the druglike, in-stock subset[53] of the ZINC 12 database,[54] consisting of ∼7 million molecules at the time of writing. Conformer generation was performed using Phase, resulting in ∼160 conformers per molecule on average. Conformers were aligned with each pharmacophore model, with exclusion volumes to prevent overlap with C3d residues.

Docking. All molecules identified in pharmacophore screens were docked to the CR2 binding region on C3d. To account for different binding site conformations of C3d, we selected five representative conformations for MD simulations for molecule docking. A total of 400 MD snapshots of C3d (200 from each trajectory) were superimposed based on Cα atoms of C3d and hierarchically clustered based on the rmsd of C3d residues involved in CR2 binding (those with >50% interaction occupancy from Figure 3d−f). The resulting dendrogram was divided into five clusters, and the medoids of these clusters were selected as representative snapshots, resulting in five C3d structures (four from the C3d−CR2 simulation and one from the free C3d simulation) with ≥1.75 Å rmsd from each other. Docking was performed using AutoDock Vina.[55] The C3d structures and ligands were processed using AutoDockTools and docked within a grid measuring 40 Å × 40 Å × 40 Å, with increased exhaustiveness parameter to enhance search accuracy within the enlarged grid. The top 20 docked poses of each molecule were returned after docking.

Scoring. All docked molecule poses were scored using the Vina scoring function. Predicted binding energies were reported for docking to each C3d conformation, and mean energies (across all C3d conformations) were used as a ranking metric. In addition, docked poses were rescreened against all pharmacophore models "in place" to identify molecules that docked in positions that overlapped with two or more pharmacophore features. Docked poses were also subjected to rmsd-based clustering to identify molecules with low-energy poses that bind in similar conformations to all C3d conformations. A combination of all scoring methods was used for selection of molecules for experimental testing.

Small Molecule Preparation. Selected druglike compounds were obtained from Enamine, Pharmeks, ChemDiv, ChemBridge, and Maybridge. Mols 4, 5, 16, 36, 42, and 68 (ChemBridge) were assessed for purity by LC−MS. The specific purities for each molecule are 91.4% (Mol4), 91.4% (Mol5), 98.4% (Mol16), 97.7% (Mol36), 95.0% (Mol42), and 88.7% (Mol68). Mols 11 and 17 (enamine) were also assessed using LC−MS and are 95% pure. Mol 22 (enamine) was assessed using NMR and stated to have 90% purity by the vendor. Mol 35 (ChemDiv) was assessed using NMR and stated to have 95% purity by the vendor. Stock solutions were prepared by dissolving molecules in DMSO to concentrations of 4 mM (with no visible precipitation) and stored at −20 °C until used. In all assays, molecules were dissolved further in appropriate aqueous buffer to minimize effects of DMSO, and DMSO (at an equivalent final concentration) was used in control samples.

Expression of Recombinant C3d. The pET15b.C3d vector (provided by Jean van den Elsen), containing the C1010A C3d mutant was transformed into *E. coli* strain BL21 (DE3), which were grown in Luria−Bertoni broth containing 100 μg/mL ampicillin and carbon source 5052 (lactose-containing autoinducer) for autoinduction of protein expression. Cultures were grown for 10−16 h at 25 °C. Subsequently, the cells were centrifuged, resuspended in 50 mM MES buffer, pH 5.5, containing DNase, RNase, protease inhibitor cocktail, and PMSF. Cells were lysed by freeze/thaw and sonication, and lysate was cleared via centrifugation and filtration. The lysate was loaded on a HiTrap SP XL column and eluted with a gradient of 0−300 mM NaCl in 50 mM MES, pH 5.5. Fractions were analyzed by SDS−PAGE, and C3d containing fractions were pooled and then loaded on a Superdex 75 26/60 HiLoad column. Once again, fractions were analyzed by SDS−PAGE, and those containing pure C3d were pooled. Activity was confirmed by binding ELISA, using known ligands Efb and Ecb. Purified C3d was aliquoted and stored at −80 °C until further use.

Microscale Thermophoresis. Direct binding of molecules was assayed using a Monolith NT.115 (NanoTemper Technologies GmbH). Purified C3d (Complement Technology, Inc.) was labeled with NT647 dye using the kit from NanoTemper Technologies and dissolved to 10 nM in MST buffer (50 mM Tris-HCl, 150 mM NaCl, 10 mM $MgCl_2$, 0.05% Tween 20) containing 5% DMSO. A dilution series of each molecule was prepared in MST buffer containing 5% DMSO and preincubated with 10 nM NT647-labeled C3d for 10 min at room temperature in the dark. Samples were loaded into hydrophilic capillary tubes, and measurements were obtained. For each molecule, reported K_D values and binding curves represent results from three independent experiments.

Absorption and Fluorescence Spectroscopy. Stock solutions of C3d-binding compounds (in DMSO) were diluted in spectroscopic grade acetonitrile (Fisher Scientific). The concentration of each sample was adjusted such that the absorption at the excitation wavelength was below 0.2, after correcting with blank acetonitrile solutions containing the same concentration of DMSO as the measured samples. The UV/visible absorption spectra (260−700 nm) were recorded on either a JASCO V-670 spectrophotometer (Tokyo, Japan) or a Shimadzu UV2450 UV−vis spectrophotometer (Tokyo, Japan), using quartz cuvettes of either 1.0 cm path length, 3.0 mL total volume (general spectra collection, quantum yield measurements) of 1.0 cm path length, 75 μL total volume (spectroscopic studies with C3d). The emission spectra were collected with either a FluoroLog-3 spectrofluorometer (Horiba-Jobin-Yvon, Edison, NJ, USA) or a Jasco FP-8300 spectrofluorometer (Tokyo, Japan). All measurements were performed at room temperature.

For spectroscopic studies with C3d, absorbance and fluorescence emission spectra were collected for each molecule at 2.5 μM concentration in PBS containing a final concentration of 5% DMSO, in the presence of 0, 3, 8, and 25 μM final concentration of recombinant C3d. For reference, spectra of samples containing the same concentrations of C3d in PBS/5% DMSO were also recorded. The corrected fluorescence spectra are reported as the difference between fluorescence intensity of a given concentration of C3d plus molecule in PBS/5% DMSO and the same concentration of C3d alone in PBS/5% DMSO. In order to compare C3d-dependent changes in fluorescence emission spectra across different molecules, we calculated the fold change in integrated fluorescence intensity as the ratio of the value at each C3d concentration divided by the value at 0 μM C3d concentration.

Fluorescence Quantum Yield Measurements. Fluorescence quantum yield values for the small molecules were calculated using one or more standard quantum yield fluorophores. Values were calculated according to

$$\Phi_S = \Phi_R \left(\frac{I_S}{I_R}\right)\left(\frac{1 - 10^{-A_R}}{1 - 10^{-A_S}}\right)\left(\frac{n_S}{n_R}\right)^2$$

where R and S subscripts denote reference compound and sample, respectively, Φ_{fl} is quantum yield, I_n is the total integrated fluorescence spectrum intensity obtained from integration of the emission spectra, A_n is sample absorbance at the excitation wavelength, and n_n is the refractive index of the solvent. Reference compounds used for calculation included naphthalene (Φ_R = 0.23 for EtOH),[56] anthracene (Φ_R = 0.27 for EtOH),[57] and coumarin 1 (Φ_R = 0.73 for EtOH).[58] Standard molecule quantum yield measurements were performed in acetonitrile.

■ ASSOCIATED CONTENT

Supporting Information

The Supporting Information is available free of charge on the ACS Publications website at DOI: 10.1021/acs.jmedchem.5b01062.

Three tables listing pharmacophore features, selected compounds fluorescence quantum yields; four figures

DOI: 10.1021/acs.jmedchem.5b01062
J. Med. Chem. 2015, 58, 9535−9545

showing structures, docked poses, and binding sites (PDF)
Molecular formula strings (CSV)

AUTHOR INFORMATION

Corresponding Author

*Phone: +1-951-827-2696. E-mail: dmorikis@ucr.edu.

Present Addresses

[⊥]R.D.G.: Department of Medical Microbiology, University Medical Center, Utrecht, Heidelberglaan 100, 3584 CX Utrecht, The Netherlands.
[#]V.N.: Department of Neurobiology, Harvard University, 220 Longwood Avenue, 315 Armenise Building, Boston, MA 02115, U.S.

Notes

The authors declare the following competing financial interest(s): Dimitrios Morikis and Ronald D. Gorham, Jr., are co-inventors in a patent application related to the work described in this paper.

ACKNOWLEDGMENTS

We kindly thank Jean van den Elsen for providing the plasmid for expression of recombinant C3d, and Piet Aerts and Maartje Ruyken for their assistance in expression and purification. We also thank Mathew Hembury, Mies van Steenbergen, and the Department of Pharmaceutics at Utrecht University for providing access to a spectrophotometer and fluorometer. This work was funded by a grant from the Beckman Initiative for Macular Research (BIMR; Grant 1404; D.M. and V.I.V.). We acknowledge instrumentation grants from the U.S. Department of the Army for the acquisition of the thermophoresis instrument (Grant W911NF-14-1-0059; D.M.), NSF CBET for the acquisition of fluorescence spectroscopy equipment (Grant 0923408; V.I.V.), and the UCR Research and Economic Development Office for matching funds (D.M., V.I.V.). R.D.G. acknowledges support from NSF EAPSI, Whitaker International Fellows and Scholars Program, Utrecht University Short-Stay Fellowship, and University of California Riverside Dissertation Year Fellowship Program. V.N. acknowledges support from NSF GRFP Grant 2011081805 and University of California Riverside Dissertation Year Fellowship Program.

ABBREVIATIONS USED

C3, the third component of the complement system; C3b, the b-fragment of C3; C3d, the d-fragment of C3; CR2, complement receptor 2; vHTS, virtual high-throughput screening; MD, molecular dynamics; rmsd, root-mean-square deviation; RCS, relaxed complex scheme

REFERENCES

(1) Walport, M. J. Complement. *N. Engl. J. Med.* **2001**, *344*, 1140−1144 (second of two parts).
(2) Wagner, E.; Frank, M. M. Therapeutic Potential of Complement Modulation. *Nat. Rev. Drug Discovery* **2010**, *9*, 43−56.
(3) Ballanti, E.; Perricone, C.; Greco, E.; Ballanti, M.; Di Muzio, G.; Chimenti, M. S.; Perricone, R. Complement and Autoimmunity. *Immunol. Res.* **2013**, *56*, 477−491.
(4) Liu, C.-C.; Manzi, S.; Kao, A. H.; Navratil, J. S.; Ahearn, J. M. Cell-Bound Complement Biomarkers for Systemic Lupus Erythematosus: From Benchtop to Bedside. *Rheum. Dis. Clin. North Am.* **2010**, *36*, 161−72−x.
(5) Thurman, J. M.; Kulik, L.; Orth, H.; Wong, M.; Renner, B.; Sargsyan, S. A.; Mitchell, L. M.; Hourcade, D. E.; Hannan, J. P.; Kovacs, J. M.; Coughlin, B.; Woodell, A. S.; Pickering, M. C.; Rohrer, B.; Holers, V. M. Detection of Complement Activation Using Monoclonal Antibodies Against C3d. *J. Clin. Invest.* **2013**, *123*, 2218−2230.
(6) Ricklin, D.; Lambris, J. D. Complement in Immune and Inflammatory Disorders: Therapeutic Interventions. *J. Immunol.* **2013**, *190*, 3839−3847.
(7) Veerhuis, R.; Nielsen, H. M.; Tenner, A. J. Complement in the Brain. *Mol. Immunol.* **2011**, *48*, 1592−1603.
(8) Sargsyan, S. A.; Serkova, N. J.; Renner, B.; Hasebroock, K. M.; Larsen, B.; Stoldt, C.; McFann, K.; Pickering, M. C.; Thurman, J. M. Detection of Glomerular Complement C3 Fragments by Magnetic Resonance Imaging in Murine Lupus Nephritis. *Kidney Int.* **2012**, *81*, 152−159.
(9) Serkova, N. J.; Renner, B.; Larsen, B. A.; Stoldt, C. R.; Hasebroock, K. M.; Bradshaw-Pierce, E. L.; Holers, V. M.; Thurman, J. M. Renal Inflammation: Targeted Iron Oxide Nanoparticles for Molecular MR Imaging in Mice. *Radiology* **2010**, *255*, 517−526.
(10) Madigan, M. C.; van den Berg, C.; Moreland, A.; Liang, J.; Lord, S.; Demir, A.; Jaiswal, S.; Jager, M. J. Macrophage Markers and C3d in the Central & Peripheral Choroid of Young, Aged and Amd Eyes. *Acta Ophthalmol.* **2012**, *90*, 0.
(11) Morrow, W. J.; Williams, D. J.; Ferec, C.; Casburn-Budd, R.; Isenberg, D. A.; Paice, E.; Snaith, M. L.; Youinou, P.; Le Goff, P. The Use of C3d as a Means of Monitoring Clinical Activity in Systemic Lupus Erythematosus and Rheumatoid Arthritis. *Ann. Rheum. Dis.* **1983**, *42*, 668−671.
(12) Mollnes, T. E.; Lea, T.; Mellbye, O. J.; Pahle, J.; Grand, Ø.; Harboe, M. Complement Activation in Rheumatoid Arthritis Evaluated by C3dg and the Terminal Complement Complex. *Arthritis Rheum.* **1986**, *29*, 715−721.
(13) Wouters, E. F. M.; Groenewegen, K. H.; Dentener, M. A.; Vernooy, J. H. J. Systemic Inflammation in Chronic Obstructive Pulmonary Disease: the Role of Exacerbations. *Proc. Am. Thorac. Soc.* **2007**, *4*, 626−634.
(14) Marc, M. M.; Kristan, S. S.; Rozman, A.; Kern, I.; Flezar, M.; Kosnik, M.; Korosec, P. Complement Factor C5a in Acute Exacerbation of Chronic Obstructive Pulmonary Disease. *Scand. J. Immunol.* **2010**, *71*, 386−391.
(15) Sargsyan, S. A.; Thurman, J. M. Molecular Imaging of Autoimmune Diseases and Inflammation. *Mol. Imaging* **2012**, *11*, 251−264.
(16) Fearon, D. T. The Complement System and Adaptive Immunity. *Semin. Immunol.* **1998**, *10*, 355−361.
(17) Toapanta, F. R.; Ross, T. M. Complement-Mediated Activation of the Adaptive Immune Responses: Role of C3d in Linking the Innate and Adaptive Immunity. *Immunol. Res.* **2006**, *36*, 197−210.
(18) Carroll, M. C.; Isenman, D. E. Regulation of Humoral Immunity by Complement. *Immunity* **2012**, *37*, 199−207.
(19) Song, H.; He, C.; Knaak, C.; Guthridge, J. M.; Holers, V. M.; Tomlinson, S. Complement Receptor 2-Mediated Targeting of Complement Inhibitors to Sites of Complement Activation. *J. Clin. Invest.* **2003**, *111*, 1875−1885.
(20) Atkinson, C.; Song, H.; Lu, B.; Qiao, F.; Burns, T. A.; Holers, V. M.; Tsokos, G. C.; Tomlinson, S. Targeted Complement Inhibition by C3d Recognition Ameliorates Tissue Injury Without Apparent Increase in Susceptibility to Infection. *J. Clin. Invest.* **2005**, *115*, 2444−2453.
(21) Rohrer, B.; Long, Q.; Coughlin, B.; Wilson, R. B.; Huang, Y.; Qiao, F.; Tang, P. H.; Kunchithapautham, K.; Gilkeson, G. S.; Tomlinson, S. A Targeted Inhibitor of the Alternative Complement Pathway Reduces Angiogenesis in a Mouse Model of Age-Related Macular Degeneration. *Invest. Ophthalmol. Visual Sci.* **2009**, *50*, 3056−3064.
(22) Fridkis-Hareli, M.; Storek, M.; Mazsaroff, I.; Risitano, A. M.; Lundberg, A. S.; Horvath, C. J.; Holers, V. M. Design and Development of TT30, a Novel C3d-Targeted C3/C5 Convertase

DOI: 10.1021/acs.jmedchem.5b01062
J. Med. Chem. 2015, 58, 9535−9545

Inhibitor for Treatment of Human Complement Alternative Pathway-Mediated Diseases. *Blood* **2011**, *118*, 4705−4713.
(23) Schmidt, C. Q.; Bai, H.; Lin, Z.; Risitano, A. M.; Barlow, P. N.; Ricklin, D.; Lambris, J. D. Rational Engineering of a Minimized Immune Inhibitor with Unique Triple-Targeting Properties. *J. Immunol.* **2013**, *190*, 5712−5721.
(24) Holers, V. M.; Rohrer, B.; Tomlinson, S. CR2-Mediated Targeting of Complement Inhibitors: Bench-to-Bedside Using a Novel Strategy for Site-Specific Complement Modulation. In *Complement Therapeutics; Advances in Experimental Medicine and Biology*; Springer US: Boston, MA, 2012; Vol. *734*, pp 137−154, DOI: 10.1007/978-1-4614-4118-2_9.
(25) Kieslich, C. A.; Morikis, D. The Two Sides of Complement C3d: Evolution of Electrostatics in a Link Between Innate and Adaptive Immunity. *PLoS Comput. Biol.* **2012**, *8*, e1002840.
(26) Nagar, B.; Jones, R. G.; Diefenbach, R. J.; Isenman, D. E.; Rini, J. M. X-ray Crystal Structure of C3d: a C3 Fragment and Ligand for Complement Receptor 2. *Science* **1998**, *280*, 1277−1281.
(27) Hammel, M.; Sfyroera, G.; Ricklin, D.; Magotti, P.; Lambris, J. D.; Geisbrecht, B. V. A Structural Basis for Complement Inhibition by Staphylococcus Aureus. *Nat. Immunol.* **2007**, *8*, 430−437.
(28) Hammel, M.; Sfyroera, G.; Pyrpassopoulos, S.; Ricklin, D.; Ramyar, K. X.; Pop, M.; Jin, Z.; Lambris, J. D.; Geisbrecht, B. V. Characterization of Ehp, a Secreted Complement Inhibitory Protein From Staphylococcus Aureus. *J. Biol. Chem.* **2007**, *282*, 30051−30061.
(29) Clark, E. A.; Crennell, S.; Upadhyay, A.; Zozulya, A. V.; Mackay, J. D.; Svergun, D. I.; Bagby, S.; van den Elsen, J. M. H. A Structural Basis for Staphylococcal Complement Subversion: X-Ray Structure of the Complement-Binding Domain of Staphylococcus Aureus Protein Sbi in Complex with Ligand C3d. *Mol. Immunol.* **2011**, *48*, 452−462.
(30) van den Elsen, J. M. H.; Isenman, D. E. A Crystal Structure of the Complex Between Human Complement Receptor 2 and Its Ligand C3d. *Science* **2011**, *332*, 608−611.
(31) Gorham, R., Jr; Kieslich, C.; Morikis, D. Complement Inhibition by Staphylococcus Aureus: Electrostatics of C3d−EfbC and C3d−Ehp Association. *Cell. Mol. Bioeng.* **2012**, *5*, 32−43.
(32) Gorham, R. D.; Rodriguez, W.; Morikis, D. Molecular Analysis of the Interaction Between Staphylococcal Virulence Factor Sbi-IV and Complement C3d. *Biophys. J.* **2014**, *106*, 1164−1173.
(33) Mohan, R. R.; Gorham, R. D.; Morikis, D. A Theoretical View of the C3d:CR2 Binding Controversy. *Mol. Immunol.* **2015**, *64*, 112−122.
(34) Clemenza, L.; Isenman, D. E. Structure-Guided Identification of C3d Residues Essential for Its Binding to Complement Receptor 2 (CD21). *J. Immunol.* **2000**, *165*, 3839−3848.
(35) Hannan, J. P.; Young, K. A.; Guthridge, J. M.; Asokan, R.; Szakonyi, G.; Chen, X. S.; Holers, V. M. Mutational Analysis of the Complement Receptor Type 2 (CR2/CD21)-C3d Interaction Reveals a Putative Charged SCR1 Binding Site for C3d. *J. Mol. Biol.* **2005**, *346*, 845−858.
(36) Isenman, D. E.; Leung, E.; Mackay, J. D.; Bagby, S.; van den Elsen, J. M. H. Mutational Analyses Reveal That the Staphylococcal Immune Evasion Molecule Sbi and Complement Receptor 2 (CR2) Share Overlapping Contact Residues on C3d: Implications for the Controversy Regarding the CR2/C3d Cocrystal Structure. *J. Immunol.* **2010**, *184*, 1946−1955.
(37) Carlson, H. A.; Masukawa, K. M.; Rubins, K.; Bushman, F. D.; Jorgensen, W. L.; Lins, R. D.; Briggs, J. M.; McCammon, J. A. Developing a Dynamic Pharmacophore Model for HIV-1 Integrase. *J. Med. Chem.* **2000**, *43*, 2100−2114.
(38) Bernard, D.; Coop, A.; MacKerell, A. D. 2D Conformationally Sampled Pharmacophore: a Ligand-Based Pharmacophore to Differentiate Delta Opioid Agonists From Antagonists. *J. Am. Chem. Soc.* **2003**, *125*, 3101−3107.
(39) Mallik, B.; Morikis, D. Development of a Quasi-Dynamic Pharmacophore Model for Anti-Complement Peptide Analogues. *J. Am. Chem. Soc.* **2005**, *127*, 10967−10976.
(40) Wong, C. F.; McCammon, J. A. Protein Flexibility and Computer-Aided Drug Design. *Annu. Rev. Pharmacol. Toxicol.* **2003**, *43*, 31−45.
(41) Nichols, S. E.; Baron, R.; Ivetac, A.; McCammon, J. A. Predictive Power of Molecular Dynamics Receptor Structures in Virtual Screening. *J. Chem. Inf. Model.* **2011**, *51*, 1439−1446.
(42) Lin, J.-H.; Perryman, A. L.; Schames, J. R.; McCammon, J. A. The Relaxed Complex Method: Accommodating Receptor Flexibility for Drug Design with an Improved Scoring Scheme. *Biopolymers* **2003**, *68*, 47−62.
(43) Amaro, R. E.; Baron, R.; McCammon, J. A. An Improved Relaxed Complex Scheme for Receptor Flexibility in Computer-Aided Drug Design. *J. Comput.-Aided Mol. Des.* **2008**, *22*, 693−705.
(44) Amaro, R. E.; Schnaufer, A.; Interthal, H.; Hol, W.; Stuart, K. D.; McCammon, J. A. Discovery of Drug-Like Inhibitors of an Essential RNA-Editing Ligase in Trypanosoma Brucei. *Proc. Natl. Acad. Sci. U. S. A.* **2008**, *105*, 17278−17283.
(45) Phillips, J.; Braun, R.; Wang, W.; Gumbart, J.; Tajkhorshid, E.; Villa, E.; Chipot, C.; Skeel, R.; Kale, L.; Schulten, K. Scalable Molecular Dynamics with NAMD. *J. Comput. Chem.* **2005**, *26*, 1781−1802.
(46) Berman, H. M.; Westbrook, J.; Feng, Z.; Gilliland, G.; Bhat, T. N.; Weissig, H.; Shindyalov, I. N.; Bourne, P. E. The Protein Data Bank. *Nucleic Acids Res.* **2000**, *28*, 235−242.
(47) MacKerell, A. D.; Bashford, D.; Bellott, M.; Dunbrack, R. L.; Evanseck, J. D.; Field, M. J.; Fischer, S.; Gao, J.; Guo, H.; Ha, S.; Joseph-McCarthy, D.; Kuchnir, L.; Kuczera, K.; Lau, F. T.; Mattos, C.; Michnick, S.; Ngo, T.; Nguyen, D. T.; Prodhom, B.; Reiher, W. E.; Roux, B.; Schlenkrich, M.; Smith, J. C.; Stote, R.; Straub, J.; Watanabe, M.; Wiórkiewicz-Kuczera, J.; Yin, D.; Karplus, M. All-Atom Empirical Potential for Molecular Modeling and Dynamics Studies of Proteins. *J. Phys. Chem. B* **1998**, *102*, 3586−3616.
(48) Humphrey, W.; Dalke, A.; Schulten, K. VMD: Visual Molecular Dynamics. *J. Mol. Graphics* **1996**, *14*, 33−38.
(49) Grant, B. J.; Rodrigues, A. P. C.; ElSawy, K. M.; McCammon, J. A.; Caves, L. S. D. Bio3d: an R Package for the Comparative Analysis of Protein Structures. *Bioinformatics* **2006**, *22*, 2695−2696.
(50) Pettersen, E. F.; Goddard, T. D.; Huang, C. C.; Couch, G. S.; Greenblatt, D. M.; Meng, E. C.; Ferrin, T. E. UCSF Chimera–a Visualization System for Exploratory Research and Analysis. *J. Comput. Chem.* **2004**, *25*, 1605−1612.
(51) Dixon, S. L.; Smondyrev, A. M.; Knoll, E. H.; Rao, S. N.; Shaw, D. E.; Friesner, R. A. PHASE: a New Engine for Pharmacophore Perception, 3D QSAR Model Development, and 3D Database Screening: 1. Methodology and Preliminary Results. *J. Comput.-Aided Mol. Des.* **2006**, *20*, 647−671.
(52) Dixon, S. L.; Smondyrev, A. M.; Rao, S. N. PHASE: a Novel Approach to Pharmacophore Modeling and 3D Database Searching. *Chem. Biol. Drug Des.* **2006**, *67*, 370−372.
(53) Lipinski, C. A. Drug-Like Properties and the Causes of Poor Solubility and Poor Permeability. *J. Pharmacol. Toxicol. Methods* **2000**, *44*, 235−249.
(54) Irwin, J. J.; Sterling, T.; Mysinger, M. M.; Bolstad, E. S.; Coleman, R. G. ZINC: a Free Tool to Discover Chemistry for Biology. *J. Chem. Inf. Model.* **2012**, *52*, 1757−1768.
(55) Trott, O.; Olson, A. J. AutoDock Vina: Improving the Speed and Accuracy of Docking with a New Scoring Function, Efficient Optimization, and Multithreading. *J. Comput. Chem.* **2010**, *31*, 455−461.
(56) Crosby, G. A.; Demas, J. N. Measurement of Photoluminescence Quantum Yields. Review. *J. Phys. Chem.* **1971**, *75*, 991−1024.
(57) Dawson, W. R.; Windsor, M. W. Fluorescence Yields of Aromatic Compounds. *J. Phys. Chem.* **1968**, *72*, 3251−3260.
(58) Jones, G.; Jackson, W. R.; Choi, C. Y.; Bergmark, W. R. Solvent Effects on Emission Yield and Lifetime for Coumarin Laser Dyes. Requirements for a Rotatory Decay Mechanism. *J. Phys. Chem.* **1985**, *89*, 294−300.

DOI: 10.1021/acs.jmedchem.5b01062
J. Med. Chem. 2015, 58, 9535−9545